Functional Sorting of Actin Isoforms in Microvascular Pericytes

David DeNofrio, Thomas C. Hoock, and Ira M. Herman

Department of Anatomy and Cellular Biology, Tufts University Schools of Medicine, Boston, Massachusetts 02111

Abstract. We characterized the form and distribution of muscle and nonmuscle actin within retinal pericytes. Antibodies with demonstrable specificities for the actin isoforms were used in localization and immunoprecipitation experiments to identify those cellular domains that were enriched or deficient in one or several actin isoforms. Living pericyte behavior was monitored with phase-contrast video microscopy before fixation to identify those cellular areas that might preferentially be stained with either of the fluorescent antiactins or phallotoxins. Antibody and phallotoxin staining of pericytes revealed that nonmuscle actin is present within membrane ruffles, pseudopods, and stress fibers. In contrast, muscle actin could be convincingly localized in stress fibers, but not within specific motile areas of pericyte cytoplasm. To confirm and quantitatively extend the results obtained by fluorescence microscopy, nonionic and ionic detergents were used to selectively extract the motile or immobilized (stress fiber-containing) regions of biosynthetically labeled pericyte cytoplasm. Immunoprecipitated actins that were present within these discrete cellular domains were subjected to isoelectric focusing in urea–polyacrylamide gels before fluorographic analysis. Scanning laser densitometry of the focused actins could not reveal any detectable α-actin within those β- and γ-actin-enriched motile regions extracted with nonionic detergents. Moreover, when pericyte stress fibers are completely dissolved by ionic detergent lysis, three actin isoforms can be quantified to be present in a ratio of 1:2.75:3 (α:β:γ). These biochemical findings on biosynthetically labeled and immunoprecipitated pericyte actins confirm the fluorescent localization studies. While the regulatory events governing this actin sorting are unknown, it seems possible that such events may play important roles in controlling cell shape, adhesion, or the promotion of localized cell spreading.

ALTHOUGH the pericyte has been described in the literature for more than a century (31), little information has been accumulated regarding its exact function within the microvasculature. Mesodermal in origin, the pericyte is found surrounding the endothelial cells of capillaries and postcapillary venules. It has been implicated in the regulation of intraocular pressures, the selectivity of the blood–brain barrier (3), and the minute-to-minute control of capillary vasomotion (34, 35). Moreover, intimate associations between the endothelial cell and the pericyte may be important in mediating the alterations in morphology, motility, and metabolism of the microvascular endothelial cells observed during angiogenesis (9, 20), in response to injury (9), or in association with the diseased state (5, 8).

Recently, vascular cell typing using antibodies specific for contractile proteins has been demonstrated to be an effective means to study the cytoskeletal constituents of large and small blood vessel cells in vitro and in situ (13, 14, 38). Previously, our laboratory has shown that retinal pericytes contain both smooth muscle and nonmuscle isoactins (14). Investigators have substantiated this by demonstrating the expression of other smooth muscle and nonmuscle cytoskeletal components in these cells (18).

Because the pericyte has been shown to possess both the smooth muscle and nonmuscle actin isotypes, we were interested to learn where these proteins were placed. Specifically, we were curious to know whether the smooth muscle and nonmuscle isoactins coassembled into the same stress fiber bundles. Studying the behavior of living pericytes made it possible to identify motile or relatively immobilized regions of the cytoplasm. Cell activity was correlated with the distribution of the isoactin pools by visualization of fluorescent phallatoxin and antibody staining, using probes specific for the different isoforms that were labeled with contrasting fluorochromes. Parallel experiments were conducted using the antibodies for immunoprecipitation of biosynthetically labeled actins that were selectively extracted from either moving cytoplasm or stress fibers. Isoelectric focusing and quantitative fluorographic analysis of these immunoprecipi-

This work was presented, in part, at the 26th annual American Society for Cell Biology meeting held December 7–11, 1986 in Washington, DC.

David DeNofrio's present address is Department of Internal Medicine, Barnes Hospital, Washington University, St. Louis, MO 63110. All reprint requests should be addressed to Ira M. Herman.

tated actin pools revealed that α-actin was present in the stress fiber fractions, but not the pseudopods and lamellae. These findings indicate that microvascular pericytes simultaneously express actins of the smooth muscle and nonmuscle gene families and that the actin isoforms are positionally sorted within the cytoplasmic matrix. Regulation of actin sorting within microvascular pericytes may be important for unique motile processes that occur during development or in association with the diseased state.

Materials and Methods

Production of Polyclonal Anti-isoactin IgG

Rabbit antiactin IgGs were produced against glutaraldehyde-fixed filaments of column-purified smooth muscle actin. Actin antibodies with defined specificities for the muscle or nonmuscle isoforms were prepared as previously described (12, 14, 14a, 30, 33).

Culture of Retinal Microvascular Pericytes

Pericytes were cultured and characterized from capillary fragments isolated from bovine retinas as previously described (11, 14).

Time-lapse Video Microscopy of Retinal Pericyte Motility In Vitro

Retinal pericytes were observed using a time-lapse videomicroscope equipped with phase-contrast optics as previously described (1, 13, 38). Briefly, pericytes attached to glass microscope coverslides were placed onto the 37°C, warmed microscope stage in a growth chamber filled with warmed and gassed media. The rate and extent of pericyte motility was ascertained from the videotape records displayed on the real-time monitor. For quantitative analysis of pericyte translocation, the image of a stage micrometer was projected onto the real-time TV monitor at the exact experimental magnification. A calibrated acetate overlay was then affixed to the monitor's surface and the position of each cell nucleus and cell border was recorded as a function of time. By plotting the intersection of the major and minor axes taken through the center of cell mass and passing through the nucleus, the translocation rates could be calculated. A statistically significant number of cells was monitored from three separate experiments ($n > 20$).

Preparation of Directly Labeled Muscle and Nonmuscle Antiactin

DEAE-Cellulose Chromatography of Antiactin IgG. Antibody labeling was carried out by a modification of the procedure of Cebra and Goldstein (7). All reactions were performed at 4°C unless otherwise indicated. IgG was precipitated from 15 ml of immune serum by titration with neutralized, saturated ammonium sulfate and added to a final concentration of 37% (wt/vol). The precipitate was centrifuged at 30,000 g_{av} for 30 min and the pellet was dissolved in 15 ml of PBS (0.015 M sodium phosphate, pH 7.5, 0.15 M sodium chloride, 0.02% sodium azide). Fractionated IgGs were then dialyzed against 6 liters (2 liters per change) of PBS. The IgG was reprecipitated, recentrifuged, and redissolved in 15 ml of PBS.

After dialysis, the IgG was fractionated on a 1.8 × 10.0-cm column of DEAE-cellulose that had been previously equilibrated with 0.01 M phosphate, pH 7.5. The antiactin IgG was applied to the column and 3.5 ml fractions were collected. Two pools of IgG were recovered. Pool I was nonadherent and passed directly through the column whereas pool II was eluted with 0.05 M sodium chloride in 0.1 M phosphate buffer, ph 7.5. The two pools were reprecipitated separately (as above), dissolved to a final IgG concentration of 10–20 mg/ml in PBS, and dialyzed against PBS. IgGs were stored at 4°C until needed.

Conjugation of Antiactin IgG with Fluorescent Dyes. TRITC and FITC (BBL Microbiology Systems, Becton, Dickinson & Co., Cockeysville, MD; Lots 12198 and 12008) conjugations were carried out using a 1-ml solution of pool I or II dialyzed against 0.01 M phosphate, pH 7.5, and then titrated to a pH of 9.5 with 0.1 M sodium hydroxide at 4°C. The IgG was then added to a reaction vessel containing 20 μg of dye per mg of IgG (6.6:1 and 8.3:1 dye to IgG molar ratios for rhodamine and fluorescein, respectively). The reaction was monitored on a pH meter for 15 min with the pH maintained at 9.5 by dropwise addition of 0.1 M sodium hydroxide. The reaction was rotated or stirred for 18 h at 4°C before chromatography on a 1.8 × 13-cm column of Sephadex G-25 equilibrated in 0.01 M phosphate, pH 7.5. The first 10 ml eluted from the Sephadex column was applied directly to a 1.8 × 10-cm column of DEAE-cellulose equilibrated in 0.01 M phosphate, pH 7.5. Dye-conjugated IgG was fractionated using stepwise salt elution. For pool I, 0.04, 0.10, and 1.00 M sodium chloride dissolved in 0.01 M phosphate, pH 7.5, was used; and for pool II, 0.04, 0.06, 0.10, and 1.00 M sodium chloride in 0.01 M phosphate, pH 7.5. Each fraction was monitored by spectrophotometry at 280 and 515 nm (for rhodamine) or 495 nm (for fluorescein conjugations). Molar ratios of dye to protein were then calculated as previously described (14a).

Affinity Fractionation of Directly Labeled Antiactins. Actin antibodies were purified after conjugation to fluorescent dyes on Sepharose 4B-actin. 0.5–1.0 mg/ml of twice-depolymerized smooth muscle (chicken gizzard) or 0.5–0.8 mg/ml nonmuscle actin (human platelet) in 0.1 M borate buffer, pH 8.8, was separately coupled to cyanogen bromide-activated Sepharose 4B at 15°C as previously described (14). 2.5 mg of conjugated immune IgG in 3.0–10.5 ml of PBS was mixed with 0.25–0.4 ml of Sepharose 4B containing 0.43–0.78 mg/ml of muscle actin or 0.74 mg/ml nonmuscle actin at pH 7.5 for 1.5–4 h at room temperature. This mixture was then poured into a 0.3 × 0.5-cm column. The unbound IgG was washed through the column at room temperature using 6 ml of PBS. These antiactin-depleted, labeled IgGs were saved and used in control experiments. The column was then washed with 10 ml of PBS. Muscle- or nonmuscle-specific antiactins were then eluted from the respective columns using 0.2 M glycine, pH 2.8. 0.5–1.0-ml fractions were collected in test tubes containing two to four drops of 0.5 M phosphate buffer, pH 7.5, which acted to neutralize the pH instantly. The fractions were then dialyzed against PBS, pH 7.5, before calculating recoveries of labeled, specific IgG and their storage at 4°C. 1.5–4% of the conjugated IgG applied to the affinity columns was recovered as affinity-purified antiactin IgGs (Table I).

Fixation, Permeabilization, and Staining of Retinal Pericytes with Actin-specific Markers

Preparation of Pericytes for Staining Experiments. For staining experiments, microvascular retinal pericytes were grown on 11 × 11-mm glass cover slips in DME supplemented with 10% calf serum. The pericytes were washed in DME for 30 s to 1 min and fixed with 4% formaldehyde in DME for 5 min. The cells were then washed three times in PBS, 0.1% BSA, and 0.02% sodium azide for 10–15 min. Cell permeabilization was accomplished in one of two ways: either by submersion for 20 s in dry ice-cold acetone; or by treatment for 90 s in a lysis buffer containing 50 mM Hepes (pH 7.1), 75 mM Pipes (pH 7.0), 1.0 mM EGTA, 5.0 mM $MgCl_2$, 0.1% Triton X-100, and 0.1% BSA at room temperature. After each permeabilization procedure the cells were washed again in PBS, 0.1% BSA, and 0.02% sodium azide. Both fixation-permeabilization methods gave equivalent staining results. Those presented herein are from the treatment of formaldehyde-fixed pericytes with the lysis buffer.

Simultaneous and Sequential Staining of Retinal Pericytes Using Fluorescent Phallatoxins and Isoactin-specific Antibodies. Sequential staining was performed using both rhodamine nonmuscle and fluorescein muscle-specific antiactins. The cells were first incubated with a 40-μl drop of fluorescein-muscle antiactin (70–80 μg/ml) for 1 h at 37°C before washing and incubation with a 40-μl drop of rhodamine nonmuscle antiactin (90 μg/ml) for 15–60 min at room temperature. After incubation with antibody, the cells were washed in PBS, 0.1% BSA, and 0.02% sodium azide and the

Table I. Recovery of Directly Labeled, Affinity-fractionated Antiactin IgG

Antiactin preparation	IgG	
	Muscle	Nonmuscle
	mg/ml	*mg/ml*
Immune IgG	10.00	10.00
Rhodamine- or fluorescein-labeled IgG with 2–5 dyes	4.68	2.17
Directly labeled affinity-purified antiactins recovered from the affinity column	0.14	0.09

coverslip mounted onto a glass microscope slide using 9:1 (vol/vol) dilution of glycerol and PBS.

Simultaneous staining experiments were performed using fluorescent phallatoxins (rhodamine-phalloidin or nitrobenzoxadiazole (NBD)[1]-phallacidin) and muscle- or nonmuscle-specific antiactin labeled with either rhodamine of fluorescein. 1 U of methanol-solubilized fluorescent phallatoxin was first evaporated under a stream of nitrogen and then resolubilized directly into the appropriate antiactin solution. Fixed and permeabilized cells were then incubated in this solution for 1 h at room temperature as previously described. Rhodamine-phalloidin, NBD-phallacidin, and the fluorescently labeled nonmuscle antiactins yielded identical actin localizations.

Indirect Staining of Microvascular Pericytes with Varying Concentrations of the Muscle or Nonmuscle Isoactin-specific Antibodies. Retinal pericytes were prepared as previously described and then incubated in 0.01, 0.10, or 1.0 mg/ml of either the muscle or nonmuscle antiactin IgG for 1 h at room temperature. Cells were washed in PBS before a 1-h incubation with 1 U of NBD-phallacidin dissolved in 50 μg/ml rhodamine-labeled goat anti-rabbit IgG.

Staining of Microvascular Pericytes with Varying Concentrations of NBD-Phallacidin. Retinal pericytes were incubated with either 1.0, 0.5, 0.25 or 0.13 U of NBD-phallacidin or rhodamine-phalloidin, for 1 h at room temperature.

Blocking Experiments Using Smooth Muscle- and Nonmuscle-specific Antibodies. Antibody blocking experiments were conducted using an excess of one or the other actin antibody solutions. For example, the pericytes were, on separate occasions, simultaneously or sequentially incubated with nonmuscle antiactin (370 μg/ml) and muscle-specific antiactin (74 μg/ml) using a 40-μl drop of each antibody separately for 1 h at room temperature. The reverse experiment was also conducted, in which the cells were first incubated with muscle-specific antibody (74 μg/ml) and then with nonmuscle antiactin (370 μg/ml).

Photomicrography. Fluorescently labeled cells were observed with phase-contrast and fluorescent optics using a Carl Zeiss, Inc. (Thornwood, NY) model IM (inverted light) microscope equipped for rhodamine and fluorescein fluorescence. Additional 510- and 580-nm barrier filters were used to avoid cross-contamination of the respective signals from the fluorescein or NBD and rhodamine fluorescence. Results from experiments were recorded through a Carl Zeiss, Inc. 1.4 numerical aperture planapochromat objective lens (63×) on Tri-X negative film (14).

Image Analysis of Antiactin and Phallatoxin-treated Pericytes

Microscope slides containing stained pericytes were viewed on a Zeiss IM-35 microscope with a 100×, NA 1.3, phase-contrast objective. For fluorescence, a 100-W mercury bulb is the light source, and standard Zeiss fluorescence filters for rhodamine and fluorescein are used. A 20× ocular is used on the video output, and a Dage-MTI, Inc. (Michigan City, IN) ISIT video camera collects the images. At this magnification, the video image of 512 pixels is 20-μm wide. Neutral density filters are placed in the path of the excitating light to reduce bleaching to a negligible level. The gain and kilovolts of the camera are adjusted manually so that the light signal is in the linear range. Images from >50 cells are collected on a Grinnell Corp. (San Jose, CA) image processor, which allows averaging of 128 frames and subtraction of a background image. For fluorescence, the background is an image of an area of the slide without cells. The adequacy of the background subtraction is checked by examining the pixel values in areas of the image without cells. Images are stored on a MicroVax computer (Digital Equipment Corp., Marlboro, MA). The ratio of light levels in NBD and rhodamine images are calculated in two ways. In the first method, the region of interest of the cell is defined, the mean fluorescence of that area is calculated for both images, and the ratio of the two means is calculated. In the second method, the computer calculates the ratio of the two images on a pixel-by-pixel basis. In this calculation, a threshold value is set so that small values, which yield spuriously high ratios, are excluded. Both methods used gave similar results.

SDS-PAGE/Western Blotting

Immunoblotting with the antiactin IgG was accomplished after SDS gel electrophoresis (21) by (*a*) equilibration of the actin-containing nitrocellulose papers in 1.5% BSA, 5.0% normal goat serum, 0.05% Tween-20, 0.9% NaCl in 0.02 M Tris-HCl, pH 7.0, for 2 h at room temperature; (*b*) washing for 15 min in three changes of 0.02 M Tris-Cl, pH 7.0, with 0.9% NaCl and 0.05% Tween-20; (*c*) overnight incubation with antiactin or control IgG (20–100 μg/ml) in antibody dilution buffer (1.5% BSA, 0.9% NaCl, 0.05% Tween-20, 0.02 M Tris-Cl, pH 7.0); (*d*) washing as in *b*; (*e*) room temperature incubation for 1.5 h in 1:200–1:500 dilution horseradish peroxidase-conjugated goat anti-rabbit IgG in antibody dilution buffer (affinity purified; Cooper Biomedical, Inc., Malvern, PA); (*f*) washing in 0.02 M Tris-Cl, pH 7.0, with 0.9% NaCl (TBS) for 15 min at room temperature; and (*g*) reaction product color development using 0.3% 4-chloro-napthol in 15% MeOH and 0.08% H_2O_2. For protein staining, Amido black (0.25% in 45% MeOH with 10% acetic acid) was used. Protein-stained and immunoblotted nitrocellulose papers were photographed using Eastman Kodak Co. (Rochester, NY) 2415 film developed in Rodinal developer (1:100) for 9 min at 20°C.

IEF-PAGE

To resolve and analyze the three major isoforms of actin present in bovine retinal pericytes, and to test the specificity and cross-reactivity of the antiactin IgGs, actins extracted and purified from cultured pericytes, chicken breast muscle, and human blood platelets were electrophoresed in ampholine-urea acrylamide gels as described in reference 17. All purified actin samples were solubilized in 8 M urea, 5% 2-mercaptoethanol, 2% NP-40, and 2% ampholines (1:4 mixture of pH 4–6:5–7; Ampholytes; Bio-Rad Laboratories, Richmond, CA) before application onto the surface of a 1.5-mm-thick slab gel of 4% acrylamide and 8 M urea, 2% ampholine mixture, 2% NP-40, 0.05% *N,N,N',N'*-tetramethylenediamine, and 0.5% ammonium persulfate. To protect the samples from the cathode buffer (0.01 M NaOH), an overlay containing 4 M urea with 1% ampholines was used. Samples were electrophoresed to the anodal solution (0.02 M H_2SO_4) for 6,500–7,000 V/hour (10, 26). Gels with isofocused actins were then (*a*) fixed for 2 h by gentle rocking in 5% perchloric acid to remove ampholines; (*b*) treated with 25% isopropyl alcohol in 10% acetic acid for 2–3 h; (*c*) equilibrated in 5% 2-mercaptoethanol, 0.1% SDS, and 0.0375 M Tris-Cl, pH 8.8, for 1 h; and (*d*) pressed against nitrocellulose paper and transferred in 25% MeOH, 5% glycine, and 25 mM Tris-Cl, pH 8.3, at 4°C and 350 mA overnight (36). The following day, the nitrocellulose was immunoblotted Western style as described above for SDS-PAGE.

Metabolic Labeling and Immunoprecipitation of Pericyte Actins

Pericytes, plated at 4–5 × 10^5 cells/well, were washed with warm PBS and fed DME deficient in methionine containing 80 μCi/ml [^{35}S]methionine (1,080 Ci/mmol; Amersham Corp. [Arlington Heights, IL], 10% fetal calf serum, and a 1× amino acid supplement containing 1% of the normal complement of methionine. Cells were then washed twice with warm PBS and extracted for timed intervals in a 0.1% Triton X-100 lysis buffer containing 40 mM Hepes (pH 7.15), 50 mM Pipes (pH 6.9), 75 mM NaCl, 1 mM $MgCl_2$, 0.5 mM EGTA, 0.1 mg/ml pepstatin, 0.1 mg/ml soybean trypsin inhibitor, with or without 0.5 mM PMSF. Duplicate samples were immediately stored on ice. After this initial extraction, the insoluble cytoskeleton, containing the stress fibers, was solubilized from the tissue-culture plates with lysis buffer including 0.5% SDS. Samples were clarified at 4°C and the supernatants were precleared in 13% goat serum with 0.3% BSA for 1 h at room temperature on a horizontal rocker. Samples were then centrifuged and clarified before making the supernates 2.5% with Protein A-Affi-gel (PA; Bio-Rad Laboratories). After an overnight incubation at 4°C, samples were once again clarified before incubation with a complex of 0.25 ml of 10% PA premixed with either of the unfractionated antiactin IgGs or the muscle-specific antiactin IgG (0.05 ml of a 10^{-4} M stock IgG solution) for a 3-h incubation at room temperature.

The pelletable PA-IgG-actin complex was centrifuged at 1,750 g_{av} for 5 min at 4°C and washed three times with a 10 mM Tris-Cl, pH 7.5, buffer containing 150 mM NaCl, 0.5% Triton X-100, and 2 mg/ml BSA. The microfuge tubes containing the immunoprecipitated PA-IgG-actin complex were then plunged into liquid nitrogen and lyophilyzed overnight. Samples were solubilized in 8 M urea containing 5% 2-mercaptoethanol, 2% NP-40, and 2% ampholytes (1:4 mixture of pH 4–6:5–7; Bio-Rad Laboratories), and electrophoresed as described in IEF-PAGE. These slab gels with radiolabeled, immunoprecipitated actins electrophoresed to their isolectric pH, were then fixed in 10% acetic acid, 30% MeOH for 1 h; impregnated with EN_3HANCE (DuPont Co., Wilmington, DE) for 1 h; rinsed with deionized water for 30 min; and dried. The dried gel was then pressed against

1. *Abbreviations used in this paper*: NBD, nitrobenzoxadiazole; PA, protein A-Affi-gel.

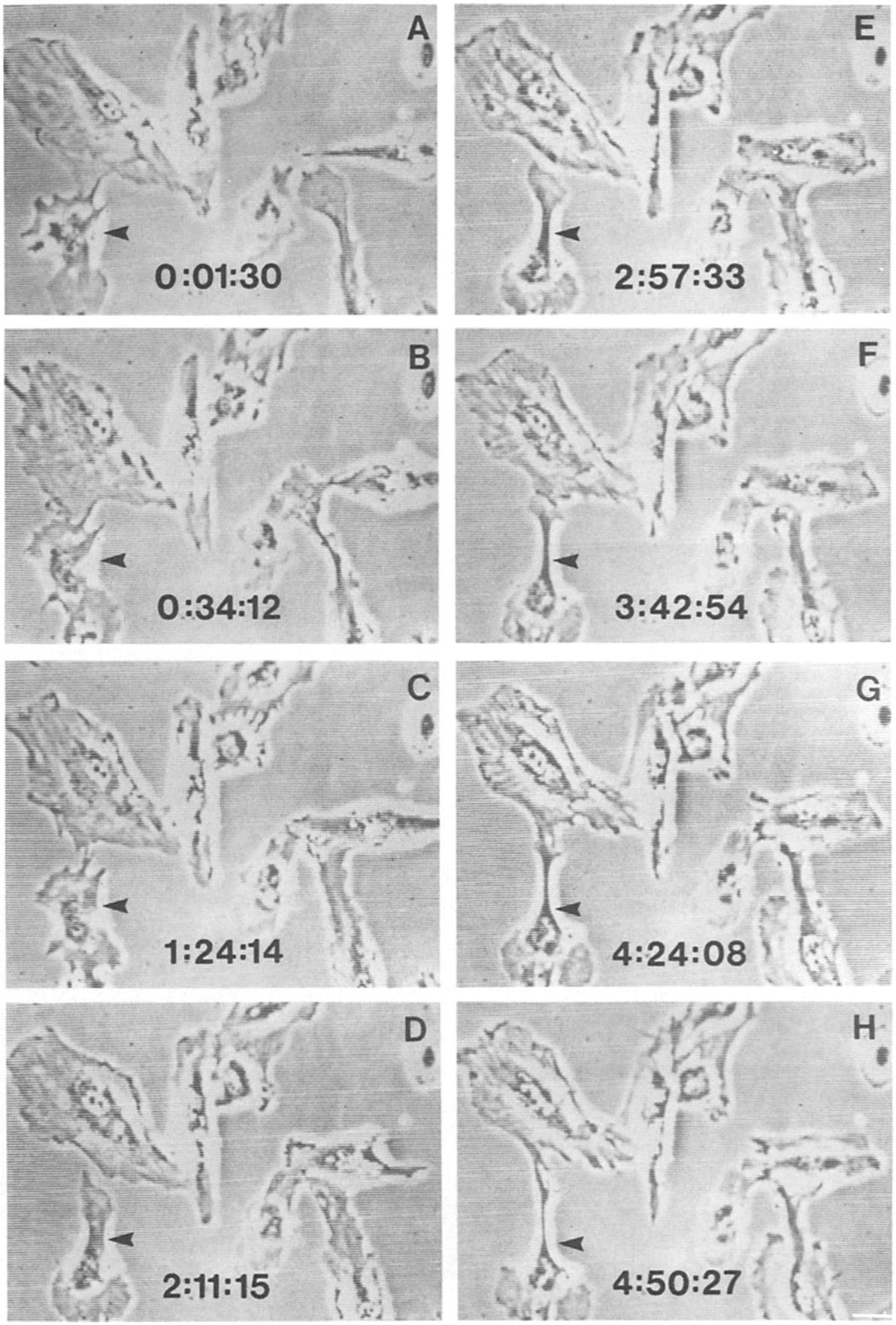

Figure 1. Time-lapse videomicroscope analysis of retinal pericyte behavior. Retinal pericytes were grown attached to glass coverslips in DME with 10% calf serum and were fitted into a culture chamber compatible for viewing under a phase-contrast light microscope (see Materials and Methods). The time (hours:minutes:seconds) appears in the lower central region of each phase-contrast image (*A–H*). Little or no pericyte translocation has occurred over the time-course of the experiment. Cellular extension and membrane activity is evident (*black arrowheads*).

x-ray film (Eastman Kodak, Co.; X-OMAT AR) and exposed at −70°C for 48 h. Peak areas of the precipitated actins were automatically digitized using a scanning laser densitometer (Ultroscan XL; LKB Instruments Inc., Gaithersburg, MD).

Results

Time-lapse Video Analysis of Retinal Pericyte Motility

When pericytes are placed into a growth chamber within a controlled environment on the stage of a time-lapse videomicroscope, a slow but deliberate motile and mitotic behavior is readily observed (Fig. 1). During interphase, the retinal pericytes are spread out and assume morphologies that occupy hundreds of square micrometers. At low population densities (10,000–30,000 cells/cm²) cell translocation is not apparent in real-time until daughter cells separate after telophase; but, at this time, pericyte migration is minimal. The migratory rates of a statistically significant number of these cells ($n > 10$) was $\sim$ 6.68 μm/h. The sequelae of pericyte extension and retraction continues until cell–cell contact is established (Fig. 1, *black arrowheads*). The relatively rapid lamellipodial extension and subsequent retraction accounts for the majority of pericyte motile activity observed in vitro.

Localization of Actin in Pericytes

Having established that pericyte motility was restricted to discrete cytoplasmic domains, we were interested to learn whether specific actin isoforms were localized in these regions of motile pericyte cytoplasm or if this actin pool was different than the actin present within immotile zones. In the rhodamine–phalloidin and fluorescein–muscle actin antibody–staining experiments, as well as in the NBD–phallacidin and rhodamine–muscle actin antibody–staining studies, there is intense phallatoxin staining of stress fiber bundles (Figs. 2 and 3). Cortical areas of the cell are well delineated with intense staining of the cell margins where some membrane ruffling is observed with time-lapse video microscopy. Additionally, there is a reticulated F-actin-rich meshwork proximal to the intensely stained membrane ruffles present in the slow spreading lamellae (Fig. 3 *B, white arrows*). Muscle actin–specific antibodies also stain the stress fibers intensely. Regardless of the antibody preparations used, each individual fiber ($n > 100$) is continuously stained and appears to possess the same overall length and width (Figs. 2 and 3). With respect to the regions of cytoplasm specifically documented as motile by time-lapse video analysis, the muscle-specific antiactins cannot be detected irrespective of the fluorophore used for labeling (Fig. 3). In experiments where the only actin probe was either the rhodamine- or the fluorescein-labeled antimuscle actin IgG, there was still no appreciable staining of the lamellar, filopodial, or membrane ruffling regions. On the other hand, retraction fibers are positive for both antibodies. To assess whether quantitative differences in staining between the antiactin antibodies and the phallatoxins could be observed, we stained pericytes with NBD–phallacidin and rhodamine-labeled muscle-specific antiactin simultaneously. Double-stained cells were observed and the respective light images stored, processed, and compared. The ratio between the two fluorescence signals was then calculated and averaged within specific regions of the cells. At the leading edges of the pericyte cytoplasm the fluorescence ratio of nonmuscle to muscle actin is 2.50. In contrast, the fluorescence intensity ratio on the stress fibers is 1.35 (Fig. 4). In experiments where the concentration of the nonmuscle antiactin exceeded the muscle antiactin by fourfold, virtually no muscle antibody staining of stress fibers could be detected (data not shown).

To test whether varying the concentration of either the muscle- or nonmuscle-specific antiactin probes altered the staining patterns obtained, we performed experiments over antibody concentrations of 0.01–1.0 mg/ml. We observed

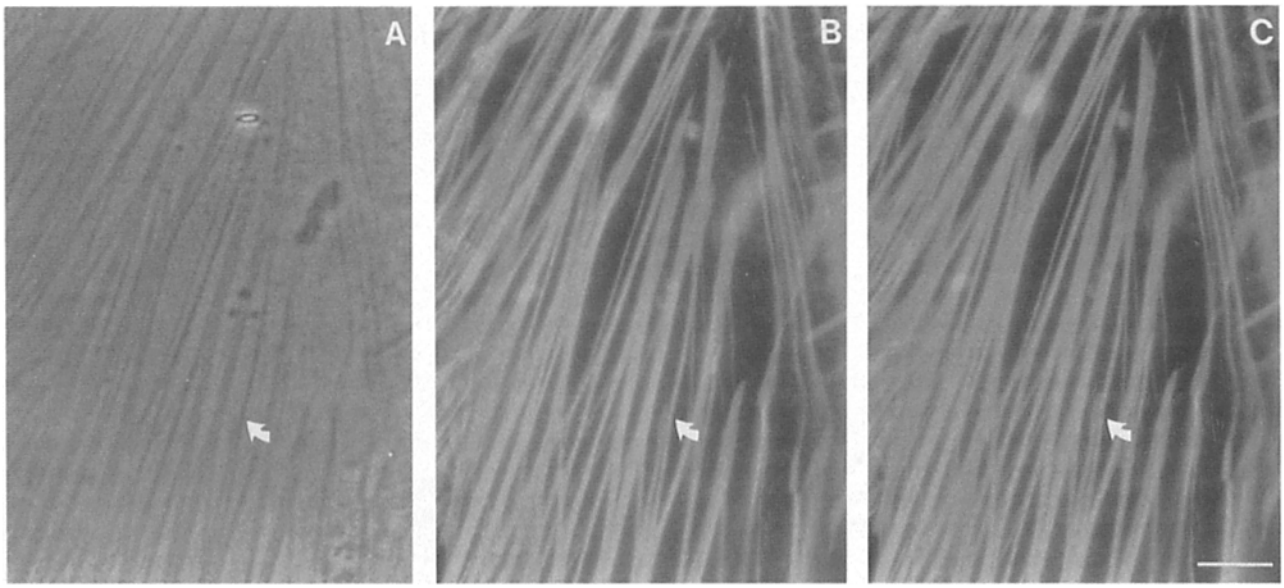

Figure 2. Simultaneous localization of pericyte isoactins with rhodamine–phalloidin and fluorescein–antimuscle actin IgG. Phase-contrast (*A*) and fluorescence (*B* and *C*) images of retinal pericytes fixed and stained with fluorescein–antimuscle actin IgG (*B*) and rhodamine–phalloidin (*C*). Note that both phallatoxins and muscle antiactin IgG yield an identical stress fiber actin localization. Bar, 10 μm.

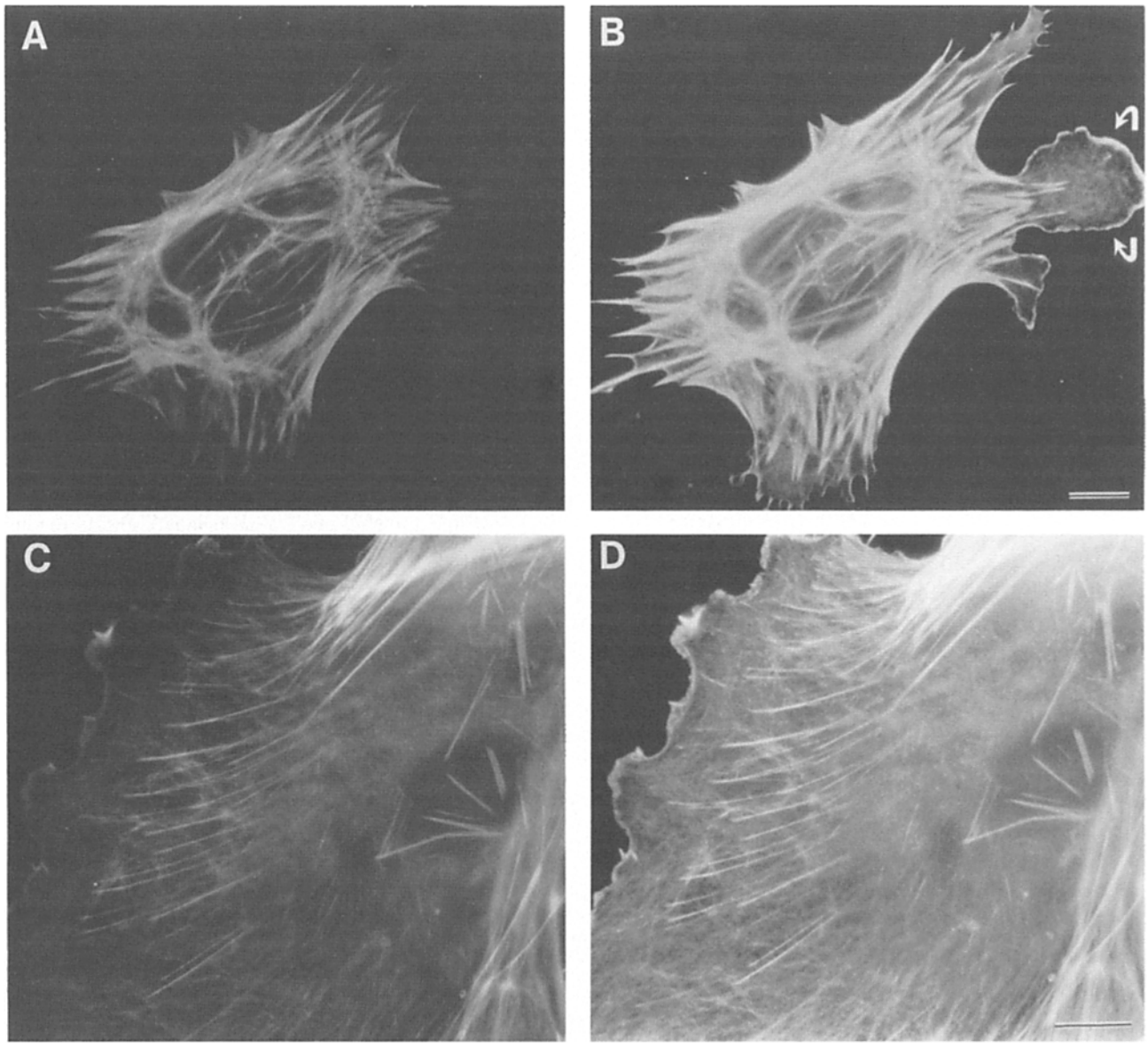

Figure 3. Sorting of isoactins in the pericyte cytoplasm. Formalin-fixed and detergent-permeabilized pericytes were incubated simultaneously with either fluorescein–antimuscle actin IgG (70–80 μg/ml) (*A*) and 1 U of rhodamine–phalloidin (*B*); or rhodamine–antimuscle actin IgG (90 μg/ml) (*C*) and 1 U of NBD–phallacidin (*D*). All isoactins are distributed on identical stress fibers. However, muscle actin is restricted from regions of motile cytoplasm (as viewed with time-lapse microscopy) such as the lamellipodia shown in *B* (*white arrows*). Bar, 10 μm.

some staining with the muscle-specific IgG in motile, lamellipodial regions of the cell only when a very high concentration of the muscle-specific antibody was used (Fig. 5, *A*, *C*, and *E*). Most probably, this is the result of a cross-reaction of the antibody with shared muscle and nonmuscle actin epitopes. At these high concentrations of IgG, we were able to observe staining within much of these cortical regions of the cell, but this is not comparable to the nonmuscle actin localization pattern (Fig. 6 *A*). In contrast, the staining of pericyte lamellae with phalloidin and/or nonmuscle-specific antiactin probes is consistently the same throughout, irrespective of antibody concentrations tested (Fig. 6). Stress fibers can be stained at all concentrations with both the muscle and nonmuscle antibodies. As we lowered the phallatoxin concentrations < 0.25 U, the staining of all cellular actin compartments was equally diminished. Similar loss of staining (below the minimum antibody concentration required for detection with immunofluorescence) occurred for each of the isoactin-specific antibodies.

Analysis of Biosynthetically Labeled Pericyte Actins by Immunoprecipitation and IEF

Simultaneous localization with isoform-specific antibodies indicated that muscle actin was restricted from slow-spreading lamellae and other motile structures, such as pseudopods. To assess whether small amounts of muscle actin were present in these motile areas, but in concentrations below the

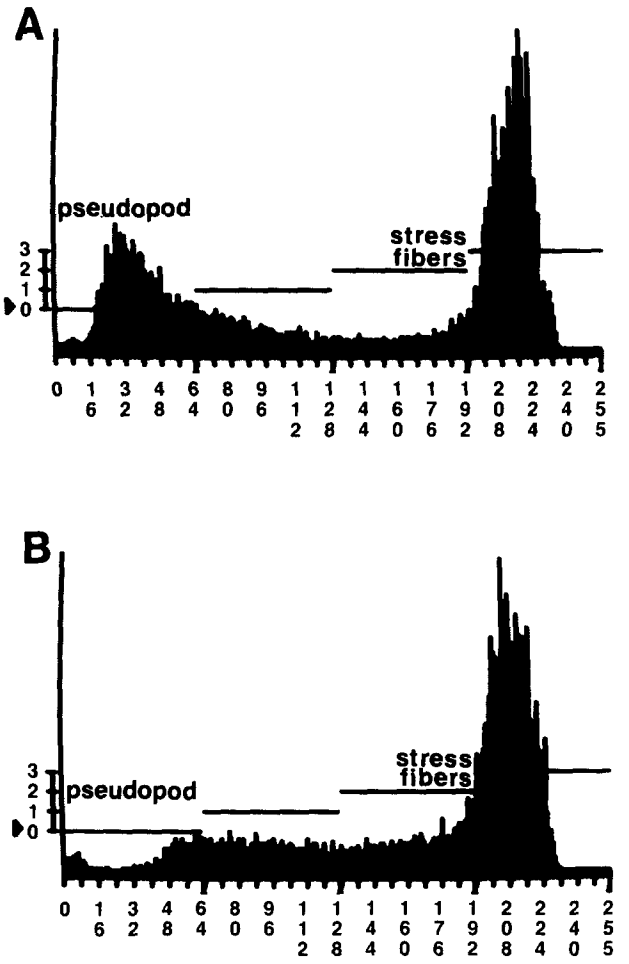

Figure 4. Representative example of the digital image analyses performed on retinal pericytes stained simultaneously, as in Fig. 3, with rhodamine-phalloidin (*A*) and antimuscle actin (*B*). The ordinate indicates the four color graphics display (*0–3*). The abscissa reveals pixel value intensity (*0–256*). The ratio image for the pseudopod and stress fiber staining is ~2.5 and 1.35, respectively.

detection limits of immunofluorescence, we devised an extraction protocol that would deplete the actin from the cortical (motile) cytoplasm while leaving the stress fiber actin pool unaltered. In this way, we could morphologically and biochemically characterize the fractional amounts of each actin that was present within each region (Figs. 7 and 8).

Using isotonic buffers containing 0.1% Triton X-100, we were able to extract actin from the pericyte cortex. Whereas, most of the lamellar anti-nonmuscle actin staining disappears within the first 5 min (Fig. 7, *C–F*; asterisk), stress fiber staining persists. Only after several minutes of detergent treatment is pericyte stress fiber staining diminished, but in discrete regions at the fibers' ends (Fig. 7 *E*, *arrowhead*). When the pericyte actins present in the detergent-soluble extracts are immunoprecipitated, focused to their isoelectric pH, and analyzed by fluorography, only the nonmuscle isoforms can be resolved (Fig. 8). In fact, over the entire time-course of extraction, i.e., when the lamellar and pseudopod actin staining completely disappears (Fig. 7), no radiolabeled muscle actin could be found in the immunoprecipitates (Fig. 8 *A*, lanes *1–3*). We digitized the radiolabeled, immunoprecipitated, and isofocused actin isoforms present in the Triton-soluble vs. insoluble fractions 10 min after lysis. This analysis revealed an order of magnitude more nonmuscle actin (both β and γ) present in the stress fiber fraction when compared to the lamellar actin fraction (c.f., Fig. 8 *A*, lanes *3* and *7*). The absence of muscle actin in the Triton X-100–solubilized extracts was confirmed by IEF in conjunction with Western blot analysis using the antiactin that recognizes all actin isoforms (Fig. 8).

Interestingly, there are subtle differences in the detectable amounts of β and γ actins present in the Triton X-100–soluble extracts when the immunoprecipitated, radiolabeled actins are compared to the Western blotted actins in the matched time points. Moreover, lysis of pericytes with 0.5% Triton X-100 yields a soluble fraction that contains roughly twice the immunoreactive amount of β- to γ-actin. Irrespective of this, muscle actin is never found in these fractions by either method (immunoprecipitation or Western blotting after IEF in urea–acrylamide slab gels; five separate experiments run in duplicate). When the Triton X-100–insoluble fraction, which contains the stress fibers, is immunoprecipitated and subjected to IEF and fluorography, all three actin isoforms can be resolved (Fig. 8 *A*, lanes *6* and *7*). Identity of the nonmuscle and muscle actin isoforms in the stress fiber–deficient and stress fiber–rich fractions were confirmed by immunoprecipitation with the nonmuscle- and muscle-specific antiactin IgGs, respectively (Fig. 8 *A*, lanes *8* and *9*). The relative amounts of radiolabeled muscle actin present within the immunoprecipitated stress fiber–rich fractions are fairly comparable if the unfractionated antiactin or the muscle-specific antiactin IgG is used for the immunoprecipitation (Fig. 8 *A*, lane *7* [actin peak area = 0.65] vs. lane *9* [actin peak area = 0.95]). Even at a time when stress fiber disassembly is complete, the α-actin is still the least abundant isoform present within the stress fiber fraction (Fig. 8 *A*, lane *7*). By scanning laser densitometry the ratio of stress fiber actin isoforms is 1:2.75:3 (α:β:γ).

Discussion

We studied retinal pericyte motility in vitro and correlated the form and distribution of the isoactin pools with cell behavior. Fluorescent phallotoxin and affinity-purified actin antibody staining revealed that the muscle and nonmuscle isoactins were distributed evenly along identical pericyte stress fibers; and muscle actin could not be localized in regions of cytoplasm documented as motile by time-lapse videomicrography. Furthermore, fluorographic analysis of isofocused immunoprecipitates derived from detergent extracts of motile pericyte cell cortex indicated that the nonmuscle (β and γ) actins, but not the muscle actin (α) were present. Analysis of the focused, radiolabeled immunoprecipitates from the stress fiber fraction, obtained at a time when the fibers are completely disassembled, revealed that the three actin isoforms were present in a ratio of 1:2.75:3 (α:β:γ).

Preparation of Antiactins Labeled with Fluorescent Dyes

While indirect immunofluorescent techniques afford specificity and sensitivity, the simultaneous localization of two or

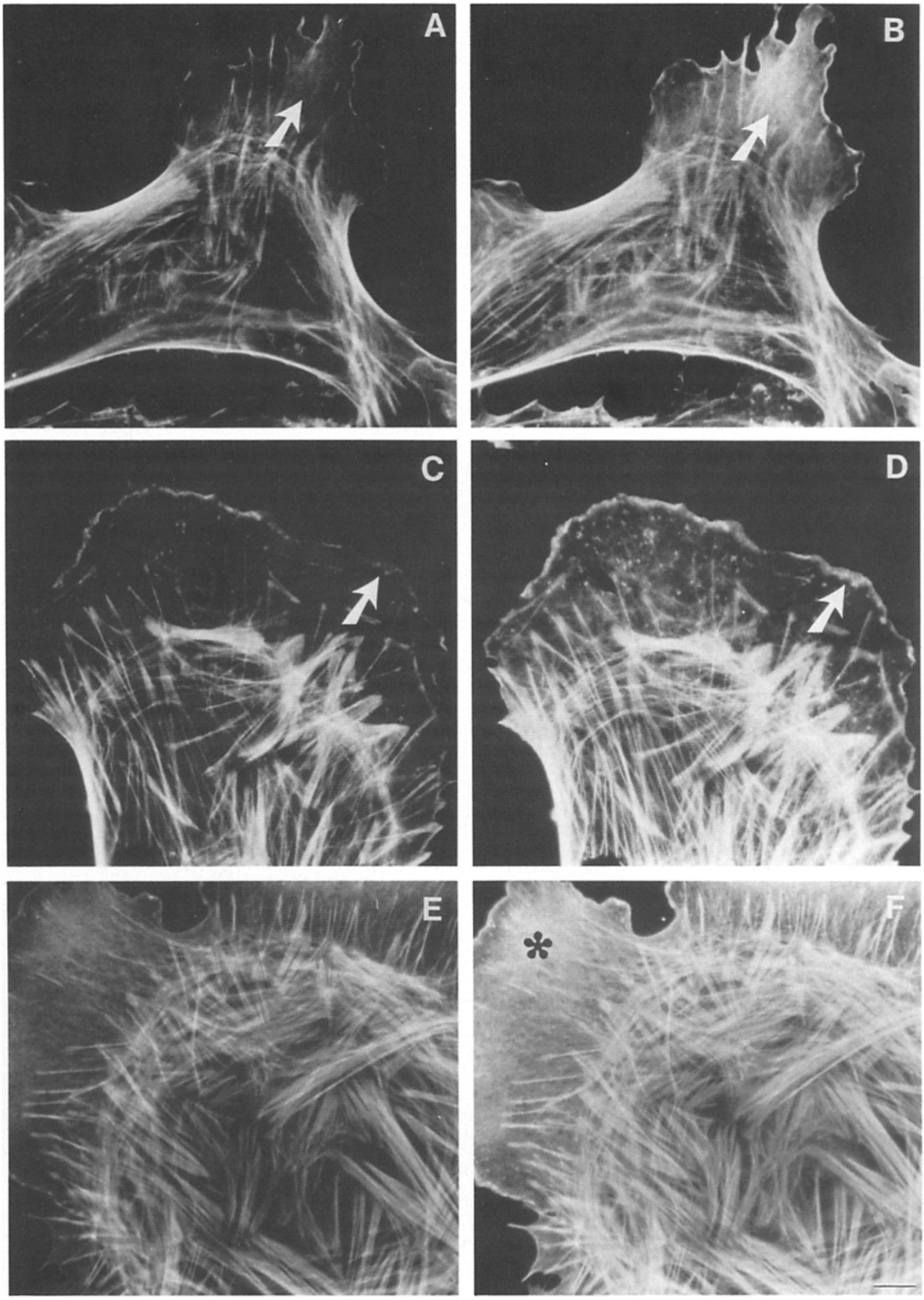

Figure 5. Muscle actin antibody concentration does not influence subcellular localization. Muscle antiactin, indirect staining (*A*, *C*, and *E*). NBD-phallacidin (*B*, *D*, and *F*). At muscle-specific antibody concentrations of 0.01 (*A*) and 0.10 mg/ml (*C*), actin staining is virtually restricted from motile regions of cytoplasm (*arrows*). At enormously high concentrations of 1.0 mg/ml (*E*), there is increased actin localization in these cortical areas of the cell (*asterisk*). Bar, 10 μm.

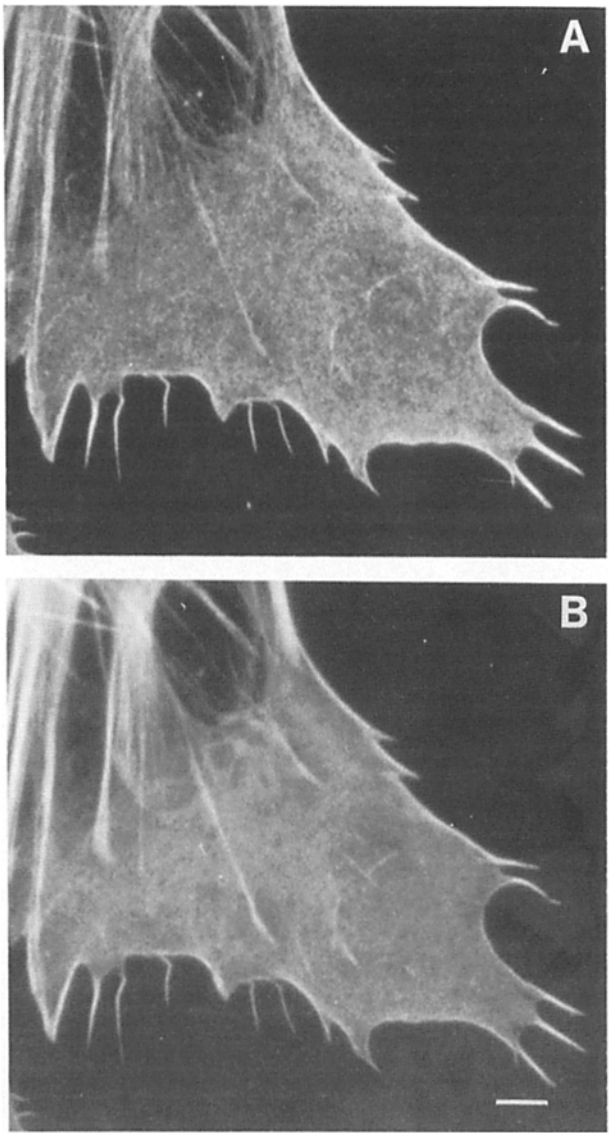

Figure 6. Nonmuscle actin localization in pericytes. Pericytes were stained indirectly using nonmuscle antiactin at concentrations of 0.01, 0.10, and 1.0 mg/ml of antibody along with 1 U of NBD-phallacidin. The lammelipodial localization is the same for both the 0.10 mg/ml nonmuscle antibody (*A*) and NBD-phallacidin (*B*) (compare with muscle localization in Fig. 5). Bar, 10 μm.

more antigens in a given specimen is difficult and cumbersome if each of the primary antibodies are elicited in the same species. However, direct conjugation of antibodies with contrasting fluorophores eliminates this potential problem. Moreover, blocking experiments can be successfully completed using the directly labeled antibody technique. This has been the case with the directly labeled, affinity-purified antiactin IgGs. One limitation that we found in the production of directly labeled antibodies is that the yield of usable probe (with an appropriate amount of conjugated dye) is low. As indicated in Table I, only 20–50% of the immune IgG pool possessed a dye/protein molar ratio that was usable for staining experiments (7). From this IgG fraction, maximally only 4% of the actin antibodies were recovered from the actin–Sepharose 4B column. In an attempt to optimize the yield of isotype-specific antiactins, the labeled antibodies were mixed with Sepharose 4B–actin under a variety of experimental conditions. Mixing together a three- to fourfold molar excess of antibodies with Sepharose 4B–actin for 1.5 h rather than 4 h yields 2.5 times more IgG if identical preparations are used. Conversely, if equimolar amounts of ligand and antibody were used, virtually no labeled antiactins could be released using either low pH or other chaotropic agents such as 4 M $MgCl_2$. Thus, the reaction time and molar ratios of antigen and antibody present could be manipulated to optimize recovery of the isotype-specific antiactins.

Regulation of Pericyte Stress Fiber Assembly

Stress fibers, consisting of a bundled network of actin filaments and associated proteins, represent a highly ordered, supramolecular array of cytoskeletal elements (6, 22, 24). This fibrous organelle is believed to be a direct or an indirect effector for the adhesion, proliferation, and migration associated with anchorage-dependent cell growth (15, 23, 38). An understanding of the mechanism(s) that controls the assembly and disassembly of stress fibers during the growth cycle may lend insight to the fundamental properties governing cell behavior.

In cells that express multiple forms of filamentous actin, it is unknown whether all of the isotypes are assembled into single actin filaments (heterotypic filaments) or if there are discrete classes of individual actin filaments (homotypic filaments) that subserve specific cell function. Microvascular pericytes, like other cells grown on planar substrates in vitro, contain many stress fibers rich in actin filaments. Time-lapse video analysis of pericyte migration revealed that these cells move at extremely slow rates concurring with previous reports that indicated a inverse relationship between stress fiber content and cell motility (Fig. 1; references 15, 16, 23). Recently, cardiac myocytes and fibroblasts isolated from chick embryos were microinjected with fluorescently labeled muscle and nonmuscle actins. Within minutes, the injected actin was shown to equilibrate with the cellular actin pool since the stress fibers as well as regions of membrane ruffles were fluorescently labeled (2, 25). These data indicate that even in slowly moving or stationary cells, stress fibers are in a dynamic state of assembly–disassembly since the injected actins equilibrate to some degree with the cytoplasmic actin pool, irrespective of isotype. We report here that in pericytes, muscle and nonmuscle actin isoforms naturally coexist on identical stress fibers. This finding indicates that stress fiber assembly can occur with multiple actin isoforms (Figs. 2–6). Yet, such an observation does not address whether (*a*) each isotype is restricted to a given actin filament, (*b*) if a specific isoform directs filament assembly uniquely, or (*c*) if specific isotypes regulate filament–filament, filament–actin-associated protein, or plasma membrane interactions. In reality, a number of stress fiber actin filament permutations could exist within cells including combinations of heterotypic and homotypic filaments of uniform or opposite polarity. Actin filament polarity within stress fibers has been examined, but the exact orientation of the individual filaments is still controversial (32). Because our studies were conducted using fluorescent antibodies and light microscopy, we cannot address these issues critically. However, the close proximity of the individual actin isoforms on a single filament is suggested by the fact that we can virtu-

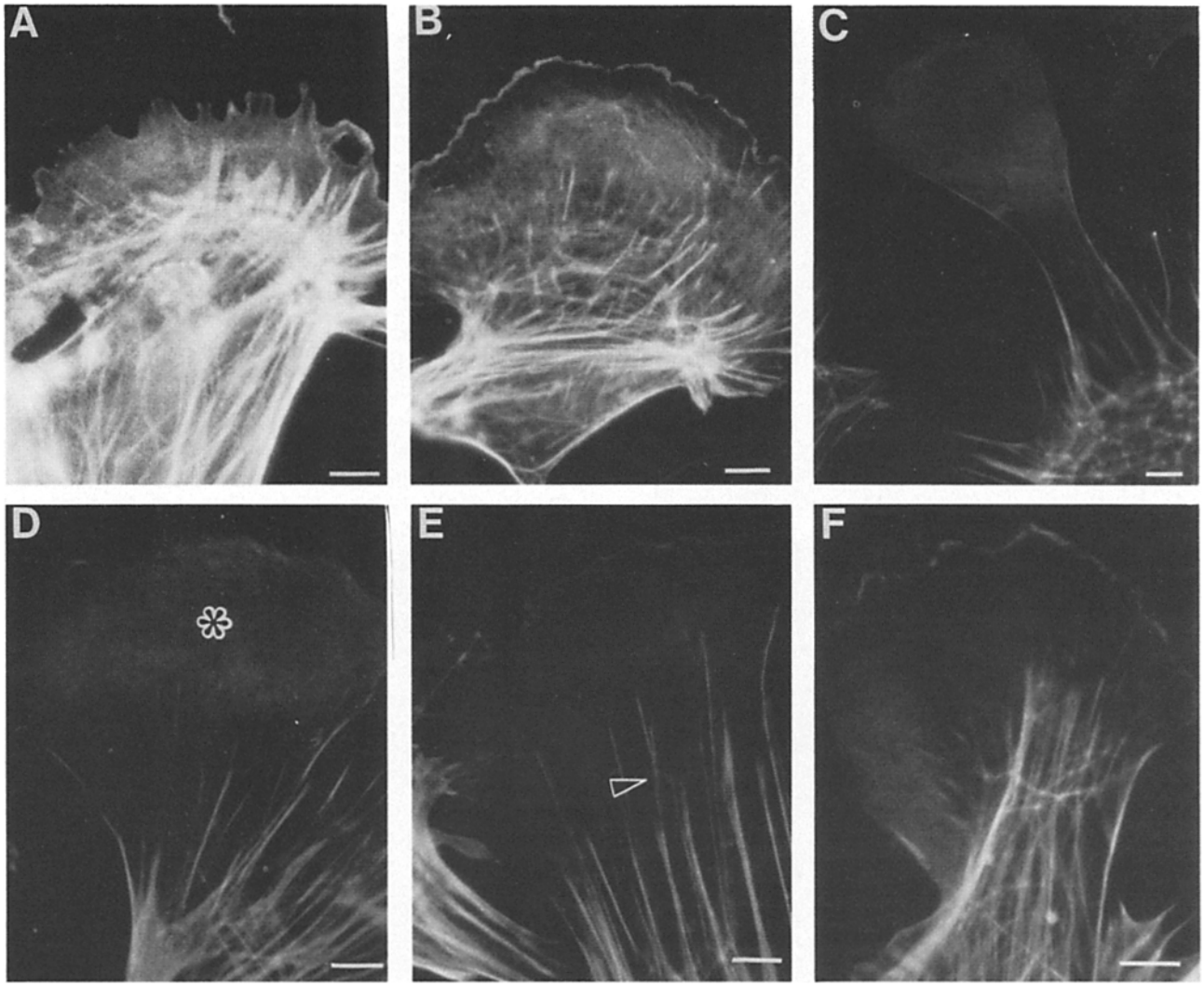

Figure 7. Selective extraction of lamellar F-actin with nonionic detergent. Fluorescence localization of rhodamine–phalloidin in retinal pericytes treated with 0.1% Triton X-100 for 0 (*A*), 1 (*B*), 2 (*C*), 4 (*D*), 8 (*E*), and 16 min (*F*). Notice the marked decrease and eventual abolition of rhodamine–phalloidin staining within the large, fan-shaped lamellae; e.g., asterisk in *D*. With increased time, the phalloidin staining at the stress fiber ends appears interrupted (*arrowhead*, *E*). Bars, 5 μm.

ally ablate muscle actin stress fiber staining with a fivefold molar excess of nonmuscle actin-specific antibodies (data not shown). Alternatively, the diminution of muscle actin-antibody staining under these experimental conditions could be explained by antibody exchange at cross-reactive muscle/nonmuscle actin epitopes.

Functional Isoactin Sorting in the Motile Cytoplasm

While our previous work (14) and the microinjection studies using fluorescent actin derivatives (2, 25) suggest that stress fiber assembly/organization is not seemingly an isoactin-specific event, functional actin sorting occurs in motile cytoplasm. The combination of time-lapse video analysis with the simultaneous and sequential staining using the labeled antiactins and the fluorescent phallotoxins clearly demonstrate that lamellae, membrane ruffles, and spikes, as well as filopodia, are rich in nonmuscle actin filaments (cf., Figs. 3 and 5–7). The actin-rich nature of these cortical regions is substantiated by the intense phallotoxin staining, a probe specific for actin filaments (37). These brightly stained regions of cytoplasm are some of the thinnest areas found in the pericyte; and, while it is difficult to estimate the local concentration of actin by immunofluorescence techniques, the combination of bright staining in attenuated cytoplasm suggests that the relative nonmuscle actin concentration is locally quite high. Our extraction studies, using 0.1% Triton X-100, indicate that these actin filaments can be readily solubilized since the phallotoxin staining can be completely eradicated (Fig. 7). Densitometric analysis of the immunoprecipitated and focused actins indicates that the β- and γ-isoforms comprise this actin pool. That higher concentrations of Triton X-100 or ionic detergents like SDS are needed to dissolve stress fibers suggests the actin filament bundles are more tightly cross-linked than those present within the lamellae. Perhaps the solubility differences observed in actin filaments from moving vs. immobilized regions of cytoplasm are the result of muscle actin interactions with specific binding proteins. Tropomyosin may be a candidate since sorting of the lower and high molecular weight tropomyosin isoforms has been

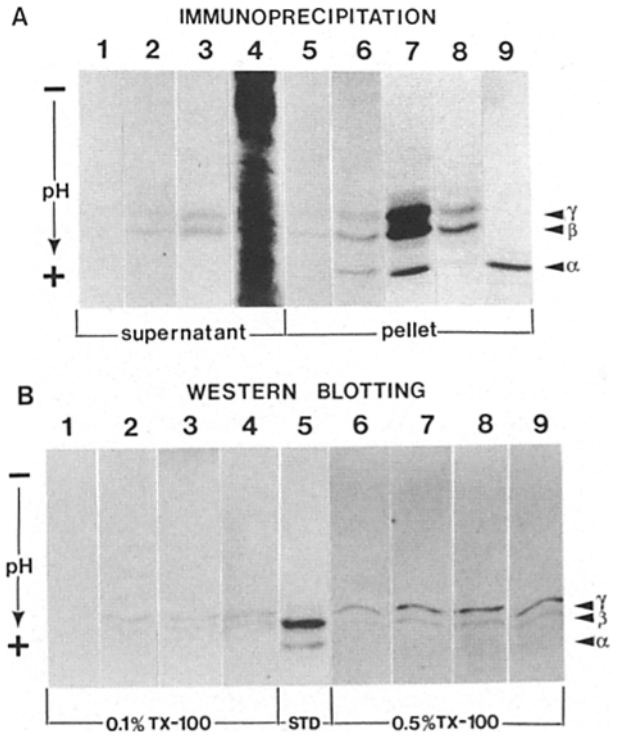

Figure 8. Electrophoretic analysis of isoactins present within discrete domains of pericyte cytoplasm. (*A*) Immunoprecipitates containing the radioactive isoactins present within the supernatant (see Fig. 7) and pellet fractions were electrophoresed to their isoelectric pH in urea–acrylamide minislab gels before fluorography. α, pI 5.1; β, pI 5.3; γ, pI 5.4. (Lanes *1–4*) Supernatant; (lanes *5–9*) pellet fractions. Extraction times: 0 (lanes *1* and *5*); 2 (lanes *2* and *6*); and 10 min (lanes *3*, *4*, and *7–9*). Notice that the unfractionated antiactin IgG only precipitates nonmuscle actins from the supernatant fraction over the experimental time-course. The immunoprecipitated sample shown in lane *3* is also shown, for comparison, before immunoprecipitation in lane *4*. In contrast to the supernatant fractions, the unfractionated antiactin IgG precipitates three actin isoforms that are present in the stress fiber (*pellet*) fraction but the nonmuscle-specific antiactin only precipitates the β- and γ-isoforms present (lane *8*). In lane *9*, the antimuscle actin IgG was used to immunoprecipitate the actin present in the fraction shown in lane *8*. Only the α-actin is precipitated and scanning laser densitometry indicates that the unfractionated and the antimuscle actin IgG precipitates nearly identical amounts of muscle actin from parallel samples (α-actin peak area = 0.65 [lane *7*]; 0.95 [lane *9*]). α-actin peak area (*B*) Western blot analysis of pericyte actins present in the supernatant fractions following Triton X-100 cell lysis for 0 (lanes *1* and *6*), 2 (lanes *2* and *7*), 5 (lanes *3* and *8*), and 10 min (lanes *4* and *9*). Note that as in the immunoprecipitation experiments, the β- and γ-actins but not the α-actins are present. The smooth muscle actin (10 μg) standard (*STD*) is shown in lane *5*.

demonstrated (23a). Noteworthy is the fact that neither high concentrations of the muscle antiactin IgG nor the nonmuscle-specific actin IgG could block the rhodamine–phalloidin or NBD–phallacidin staining whether the antibody was conjugated with either rhodamine or fluorescein (i.e., rhodamine–muscle antiactin or rhodamine–nonmuscle antiactin used in combination with NBD–phallacidin; or fluorescein–muscle antiactin used in combination with rhodamine–phalloidin).

Investigators have tried to relate the expression of isoactins in cultured cells with differentiation (4, 19), proliferation (7a, 29), and subcellular function (30). Recently, other workers have used polyclonal and monoclonal actin antibodies combined with immunoblotting (27) or fluorescence microscopy to demonstrate that the β- and γ-isoforms are not differentially sorted in all cultures of vertebrate nonmuscle cells tested (28). These data concur with our localization of nonmuscle actin within the stress fibers and motile regions of pericytes and the cortex of vascular smooth muscle cells (14). The mechanisms that regulate the recruitment of muscle actin into the stress and retraction fiber pools, but prevent its accumulation in the regions of slowly spreading cytoplasm, are currently unknown. A number of possibilities exist including (*a*) the presence of membrane- or stress fiber–associated actin-binding proteins that restrict the isoactins in these cellular domains; (*b*) sequence microheterogeneities or posttranslational modifications of the isoactins; or (*c*) subcellular control of the position and stability of isoactin mRNAs. Studies are now focused on revealing the molecular mechanisms that influence cytoskeletal protein expression and sorting in microvascular pericytes.

We thank John Cooper and Elliot Elson, Washington University School of Medicine (St. Louis, MO), for performing the image analysis of antiactin- and phallotoxin-treated pericytes.

This work was supported in part by a Tufts University Student Research Award to D. DeNofrio and an American Heart Association Established Investigatorship Award and National Institutes of Health grant HL 35570 to I. M. Herman.

Received for publication 9 January 1989 and in revised form 15 February 1989.

References

1. Adams, R. J., and T. D. Pollard. 1986. Propulsion of organelles isolated from Acanthamoeba along actin filaments by myosin-I. *Nature (Lond.).* 322:754–756.
2. Amato, P. A., and D. L. Taylor. 1986. Probing the mechanism of fluorescently labeled actin into stress fibers. *J. Cell Biol.* 102:1074–1084.
3. Broadwell, R. D., and M. Salcman. 1981. Expanding the definition of the blood-brain barrier to protein. *Proc. Natl. Acad. Sci. USA.* 78:7820–7824.
4. Bulinski, J. C., S. Kumar, K. Titani, and S. D. Hauschka. 1983. Peptide antibody specific for the amino terminus of skeletal muscle alpha-actin. *Proc. Natl. Acad. Sci. USA.* 50:1506–1510.
5. Buzney, S. M., R. N. Frank, S. D. Varma, T. Tanishima, and K. H. Gabbay. 1977. Aldose reductase in retinal mural cells. *Invest. Ophthalmol. & Visual Sci.* 16:392–396.
6. Byers, H. R., G. E. White, and K. Fujiwara. 1984. Organization and function of stress fibers in cells in vitro and in situ. A review. *Cell Muscle Motil.* 5:83–137.
7. Cebra, J. J., and G. Goldstein. 1965. Chromatographic purification of tetramethylrhodamine-immune globulin conjugates and their use in the cellular localization of rabbit gamma globulin polypeptide chains. *J. Immunol.* 95:230–245.
7a. Clowes, A. W., M. M. Clowes, O. Kocher, P. Ropraz, C. Chaponnier, and G. Gabbiani. 1988. Arterial smooth muscle cells in vivo: relationship between actin isoform expression and mitogenesis and their modulation by heparin. *J. Cell Biol.* 107:1939–1945.
8. Cogan, D. G., D. Toussaint, and T. Kuwabara. 1961. Retinal vascular patterns. IV. Diabetic retinopathy. *Arch. Ophthalmol.* 66:366–378.
9. Crocker, D. J., T. M. Murad, and J. C. Geer. 1970. Role of the pericyte in wound healing. An ultrastructural study. *Exp. Mol. Pathol.* 13:51–65.
10. Garrels, J. I., and W. Gibson. 1976. Identification and characterization of multiple forms of actin. *Cell.* 9:795–805.
11. Gitlin, J. D., and P. A. D'Amore. 1983. Culture of retinal capillary cells using selective growth media. *Microvasc. Res.* 26:74–80.
12. Herman, I. M. 1988. Developing probes and methods for morphological and biochemical analyses of cytoskeletal elements in vascular cells. *CRC Crit. Rev. Anat. Sci.* 1:133–148.
13. Herman, I. M., and P. A. D'Amore. 1984. Capillary endothelial cell migration: loss of stress fibres in response to retina-derived growth factor. *J.*

Muscle Res. Cell Motil. 5:697–709.
14. Herman, I. M., and P. A. D'Amore. 1985. Microvascular pericytes contain muscle and nonmuscle actins. *J. Cell Biol.* 101:43–52.
14a. Herman, I. M., and T. D. Pollard. 1979. Comparison of purified anti-actin and fluorescent-heavy meromyosin staining patterns in dividing cells. *J. Cell Biol.* 80:509–520.
15. Herman, I. M., N. J. Crisona, and T. D. Pollard. 1981. Relation between cell activity and the distribution of cytoplasmic actin and myosin. *J. Cell Biol.* 90:84–91.
16. Herman, I. M., T. D. Pollard, and A. J. Wong. 1982. Contractile proteins in endothelial cells. Endothelium. *Ann. NY Acad. Sci.* 401:50–60.
17. Hoefer Scientific Instrument Catalogue. 1986. Exercise in electrophoretic transfer of isofocused gels to nitrocellulose and immunostaining of nitrocellulose blots. Hoefer Scientific Instruments, San Francisco, CA. 148–151.
18. Joyce, N. C., M. F. Haire, and G. E. Palade. 1985. Contractile proteins in pericytes. II. Immunocytochemical evidence for the presence of two isomyosins in graded concentrations. *J. Cell Biol.* 100:1387–1395.
19. Kuroda, M. 1985. Change of actin isomers during differentiation of smooth muscle. *Biochim. Biophys. Acta.* 843:208–213.
20. Kuwabara, T., and D. G. Cogan. 1963. Retinal vascular patterns. VI. Mural cells of the retinal capillaries. *Arch. Ophthalmol.* 69:492–502.
21. Laemmli, U. K. 1970. Cleavage of structural proteins during the assembly of the head of Bacteriophage T_4. *Nature (Lond.).* 227:680–685.
22. Lark, M. W., J. Laterra, and L. A. Culp. 1985. Close and focal contact adhesions of fibroblasts to a fibronectin-containing matrix. *Fed. Proc.* 44:394–403.
23. Lewis, L., J. M. Vera, D. Levinstone, S. Sher, L. Mark, and E. Bell. 1982. The relationship of fibroblast translocations to cell morphology and stress fibre density. *J. Cell Sci.* 53:21–36.
23a. Lin, J.-C., T. E. Hegmann, and J. L.-C. Lin. 1988. Differential localization of tropomyosin isoforms in non-muscle cells. *J. Cell Biol.* 107: 563–572.
24. Mangeat, P., and K. Burridge. 1984. Actin-membrane interaction in fibroblasts: what proteins are involved in this association? *J. Cell Biol.* 99(Suppl.):95s–103s.
25. McKenna, N., J. B. Meigs, and Y. L. Wang. 1985. Identical distribution of fluorescently labeled brain and muscle actins in living cardiac fibroblasts and monocytes. *J. Cell Biol.* 100:292–296.
26. O'Farrell, P. H. 1975. High resolution two dimensional electrophoresis of proteins. *J. Biol. Chem.* 250:4007–4021.
27. Otey, C. A., M. H. Kalnoski, and J. C. Bulinski. 1987. Identification and quantification of actin isoforms in vertebrate cells and tissues. *J. Cell. Biochem.* 34:113–124.
28. Otey, C. A., M. H. Kalnoski, J. L. Lessard, and J. C. Bulinski. 1986. Immunolocalization of the gamma isoform of nonmuscle actin in cultured cells. *J. Cell Biol.* 102:1726–1737.
29. Owens, G. K., A. Loeb, D. Gordon, and M. M. Thompson. 1986. Expression of smooth muscle-specific alpha-isoactin in cultured vascular smooth muscle cells: relationship between growth and cytodifferentiation. *J. Cell Biol.* 102:343–352.
30. Pardo, J. V., M. F. Pittenger, and S. W. Craig. 1983. Subcellular sorting of isoactins: selective association of actin with skeletal muscle mitochondria. *Cell.* 32:1093–1103.
31. Rouget, C. 1879. Sur la contractile des capillares sanguines. *C. R. Acad. Sci.* 88:916–918.
32. Sanger, J. M., and J. W. Sanger. 1980. Banding and polarity of actin filaments in interphase and cleaving cells. *J. Cell Biol.* 86:568–575.
33. Spudich, J. A., and S. Watt. 1971. The regulation of rabbit skeletal muscle contraction. I. Biochemical studies of the interaction of the tropomyosin-troponin complex with actin and the proteolytic fragments of myosin. *J. Biol. Chem.* 246:4866–4871.
34. Tilton, R. G., C. Kilo, and J. R. Williamson. 1979. Pericyte-endothelial relationships in cardiac and skeletal muscle capillaries. *Microvasc. Res.* 18:325–335.
35. Tilton, R. G., C. Kilo, J. R. Williamson, and D. W. Murch. 1979. Differences in pericyte contractile function in rat cardiac and skeletal muscle microvasculatures. *Microvasc. Res.* 18:336–352.
36. Towbin, H., T. Staehelin, and J. Gordon. 1979. Electrophoretic transfer of proteins from polyacrylamide gels to nitrocellulose sheets: procedure and some applications. *Proc. Natl. Acad. Sci. USA.* 76:4350–4354.
37. Wieland, T., and H. Faulstich. 1978. Amatoxins, phallotoxins, phallolysin, and antamanide: the biologically active components of poisonous *Amanita* mushrooms. *CRC Crit. Rev. Biochem.* 5:185–260.
38. Young, W. C., and I. M. Herman. 1985. Extracellular matrix modulation of endothelial cell shape and motility following injury in vitro. *J. Cell Sci.* 73:19–32.